# Sequence-Selective Recognition of Duplex DNA through Covalent Interstrand Cross-Linking: Kinetic and Molecular Modeling Studies with Pyrrolobenzodiazepine Dimers†

Melissa Smellie,‡ Deravander S. Bose,§ Andrew S. Thompson,§ Terence C. Jenkins,|| John A. Hartley,‡ and David E. Thurston*,§

*Cancer Research UK Drug-DNA Interactions Research Group, Department of Oncology, Royal Free & University College Medical School, UCL, 91 Riding House Street, London W1W 7BS, U.K., Cancer Research UK Gene Targeted Drug Design Research Group, The School of Pharmacy, University of London, 29/39 Brunswick Square, London WC1N 1AX, U.K., and Yorkshire Cancer Research Laboratory of Drug Design, Tom Connors Cancer Research Centre, University of Bradford, All Saints Road, Bradford, West Yorkshire BD7 1DP, U.K.*

*Received February 24, 2003; Revised Manuscript Received May 2, 2003*

ABSTRACT: Members of a homologous series of pyrrolo[2,1-*c*][1,4]benzodiazepine (PBD) dimers with C8-O-$(CH_2)_n$-O-C8′ diether linkages ($n = 3-6$ for **2a**−**d**, respectively) have been studied for their ability to interact with oligonucleotide duplexes containing potential target binding sites. The results confirm earlier predictions that the $n = 3$ analogue (**2a**, DSB-120) will covalently bind to a 5′-Pu-***G****ATC*-Py sequence by cross-linking opposite-strand guanines separated by 2 bp. Preference for this DNA sequence is shown using oligonucleotides with altered bases between and/or flanking these guanines. The more extended PBD dimer **2c** ($n = 5$) can span an extra base pair and cross-link the 5′-Pu-***GA(T/A)TC***-Py sequence. The ability of each homologue to cross-link linear plasmid DNA has been determined, with a rank order that correlates with the reported order of *in vitro* cytotoxicity: $n = 3$ (**2a**) > $n = 5$ (**2c**) > $n = 6$ (**2d**) > $n = 4$ (**2b**). The $n = 3$ homologue (**2a**) is >300-fold more efficient at cross-linking DNA than the clinically used cross-linking agent melphalan under the same conditions. Kinetic studies reveal that the $n = 3$ and 5 dimers achieve faster cross-linking to plasmid DNA (108 and 81% cross-linking $h^{-1}$ $\mu M^{-1}$ at 37 °C, respectively), whereas the $n = 4$ and 6 homologues are significantly less efficient at 10.3 and 23% cross-linking $h^{-1}$ $\mu M^{-1}$, respectively. Alternating activity for the odd *n* and even *n* dimers is probably due to configurational factors governed by the spatial separation of the PBD subunits and the flexible character of the tethering linkage. Molecular modeling confirms the order of cross-linking reactivity, and highlights the role of linker length in dictating sequence recognition for this class of DNA-reactive agent.

Pyrrolo[2,1-*c*][1,4]benzodiazepine (PBD)[1] dimers are synthetic sequence-selective interstrand DNA minor groove cross-linking agents developed from the monomeric anthramycin family of naturally occurring antitumor agents (*1*). The tricyclic PBD subunit incorporates a chiral center at the C11a position and a DNA-reactive imine moiety at the N10 and C11 positions (e.g., DC-81 in Figure 1). The molecules adopt the appropriate three-dimensional shape to fit into the minor groove of double-stranded (duplex) DNA such that the imine can effect subsequent alkylation at the exocyclic N2 of a guanine base. PBD monomers typically span ∼3 bp of DNA with an alkylating preference for 5′-A**G**A sequences. Furthermore, PBD monomers can inhibit both endonuclease (*2*) and RNA polymerase (i.e., transcription) (*3*) enzymes in

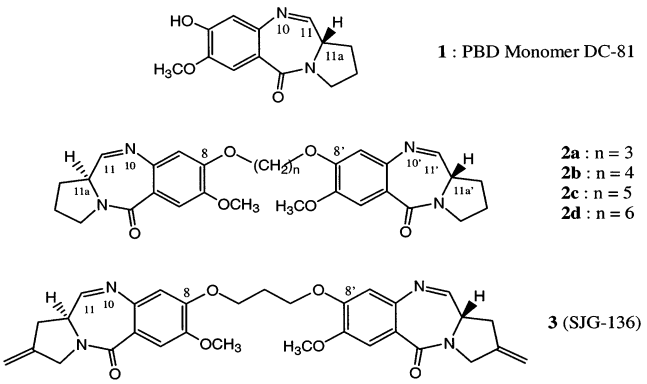


FIGURE 1: Structures of a PBD monomer (**1**, DC-81) and the homologous synthetic PBD dimer series (**2a**−**d**). PBD dimer **3** (SJG-136) has been selected for clinical trial.

† This work was supported by Cancer Research UK (Grants C180/A1060, SP1938/0402, SP1938/0201, SP1938/0301, and SP2000/0402 to D.E.T., J.A.H., and T.C.J.) and Yorkshire Cancer Research (to T.C.J.). The UK Research Council is thanked for an Earmarked QUOTA Award (91306038 to M.S.) and a Molecular Recognition Initiative postdoctoral fellowship (GR/F52675 to D.S.B.). The Royal Pharmaceutical Society of Great Britain is acknowledged for a studentship (to A.S.T.).

* To whom correspondence should be addressed: The School of Pharmacy, University of London, 29/39 Brunswick Square, London WC1N 1AX, U.K. Phone: [044] (0)207 753 5931. Mobile phone: [044] (0)7976-801535. E-mail: david.thurston@ulsop.ac.uk. Fax: [044] (0)-207-753-5935.

‡ Royal Free & University College Medical School.

§ University of London.

|| University of Bradford.

[1] Abbreviations: MD, molecular dynamics; MM, molecular mechanics; PBD, pyrrolo[2,1-*c*][1,4]benzodiazepine; SAR, structure−activity relationship.

10.1021/bi034313t CCC: $25.00 
Published on Web 06/17/2003

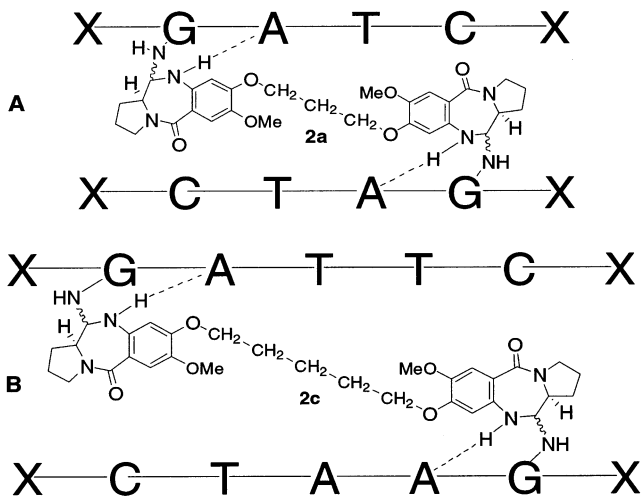


FIGURE 2: Proposed mechanism for interstrand cross-linking of DNA by (A) PBD dimer **2a** and (B) PBD dimer **2c**. The sequence selectivity is partly due to (a) the covalent bonds between the C11 positions of the PBD moieties and the exocyclic N2 groups of the guanines on opposite strands (shown as wavy lines) and (b) the hydrogen bonds (shown as dashed lines) formed between the N10 protons of the PBD moieties and the ring nitrogen acceptors of the adenines adjacent to the covalently modified guanines. X is used to denote any flanking base.

a sequence-dependent manner. A number of synthetic routes to PBDs have been developed (*4*, *5*), and their structure−activity relationships (SARs) are now well-understood (*6*−*8*). Such agents are currently being used as part of a gene targeting program designed to exploit their inherent reactivity toward embedded biologically significant G-containing DNA sequences (*9*).

The first C8/C8′-linked PBD dimer (**2a** in Figure 1, DSB-120) was reported in 1992 where two DC-81 subunits are joined through the C8 positions of their aromatic A rings through an inert propyldioxy [i.e., -O-$(CH_2)_3$-O- diether] linker (*10*). Dimeric homologues **2b**−**d** [-O-$(CH_2)_n$-O-, where $n = 4-6$, respectively] were later synthesized (*11*), and their relative cytotoxic potencies and DNA cross-linking efficiencies reported (*12*), together with their cellular pharmacology (*13*). Extensive molecular modeling and an NMR structural study showed that PBD dimer **2a** spans a ∼6 bp tract in a targeted DNA duplex (Figure 2), with a cross-linking reactivity preference for 5′-Pu-***G****ATC*-Py sequences (*14*−*16*). However, while **2a** shows potent *in vitro* cytotoxicity toward a panel of human cancer cell lines (*10*, *12*), it was found to lack significant *in vivo* antitumor activity (*17*). Derivatives with either different C2/C2′ substitution and/or unsaturation in the pyrrolidine C rings have since been evaluated, and a firm basis for the observed SAR has been established (*18*). On this basis, a C2/C2′ *exo*-unsaturated analogue SJG-136 (**3**) with an equivalent $n = 3$ diether linkage has been identified that affords significant *in vitro* (*19*, *20*) and *in vivo* activity, and this molecule has been selected for clinical trials.

The biological activity of PBD dimers is thought to be a consequence of their sequence-selective interaction with genomic regions that contain an overabundance of relevant binding sites (*21*, *22*), a concept that is now being applied to other sequence-selective binding agents (*23*−*25*). Thus, the DNA recognition profile of simple PBD monomers and their derived synthetic dimers offers a means of targeting

**Oligonucleotide Structure** **Generalized Sequence**

| | | | |
|---|---|---|---|
| **A.** | | 5′-pu-***G***-pu | |
| **B.** | | 5′-pu-***G***-pu-py-C-py | (pu-***G***-pu) |
| | | py-C-py-pu-***G***-pu-5′ | (pu-***G***-pu) |
| **C.** | **Oligo-1** | 5′-CIC-***G****ATC*-ICG | (py-***G***-pu) |
| | | GCI-*CTA****G***-CIC-5′ | (py-***G***-pu) |
| | **Oligo-2** | 5′-CIC-***G****TAC*-ICG | (py-***G***-py) |
| | | GCI-*CAT****G***-CIC-5′ | (py-***G***-py) |
| | **Oligo-3** | 5′-TATA-***G****ATC*-TATA | (pu-***G***-pu) |
| | | ATAT-*CTA****G***-ATAT-5′ | (pu-***G***-pu) |
| | **Oligo-4** | 5′-TATA-***G****ATTC*-TATA | (pu-***G***-pu) |
| | | ATAT-*CTAA****G***-ATAT-5′ | (pu-***G***-pu) |

FIGURE 3: (A) General preferred DNA alkylation site for a PBD monomer. (B) Preferred DNA cross-linking site proposed for dimer **2a** (*14*−*16*). (C) Oligonucleotide DNA duplexes containing a single site for cross-linking by the PBD dimers. The Oligo-1 duplex was used previously for NMR and modeling studies with **2a**, where the flanking rather than strand-terminating guanine bases had been replaced with inosine. Oligo-2 is similar to Oligo-1, but the two core base pairs are reversed. Oligo-3 and Oligo-4 contain the optimum cross-linking sequences predicted by molecular modeling for **2a** ($n = 3$) and **2c** ($n = 5$), respectively.

genomic DNA sequences for potential therapeutic control of diseases.

To confirm the base pair span and sequence-selectivity towards duplex-form DNA, a series of radiolabeled oligonucleotides was selected (Figure 3C) to enable a comparison of reactivity and cross-linking potential within the homologous PBD dimer series **2a**−**d** ($n = 3-6$, respectively, in Figure 1). The results confirm that the $n = 3$ and 5 (i.e., odd $n$) homologues are the most efficient cross-linking agents, and show that **2a** prefers a 5′-**G**ATC sequence but cannot tolerate an additional base pair between the two separated guanines on adjacent strands. However, the more extended PBD dimer **2c** ($n = 5$) favors a longer 5′-**G**AATC (≡ 5′-**G**ATTC) sequence but can also covalently cross-link the short 5′-**G**ATC site, albeit less efficiently, presumably through a folded-linker conformation adopted by the bound ligand.

## MATERIALS AND METHODS

*PBD Compounds and Solutions.* All PBD dimers were synthesized as described previously (*11*, *12*). Drug solutions were prepared in HPLC-grade methanol prior to use; the methanol concentration in working DNA/drug mixtures was <0.5% (v/v).

*Quantitation of DNA Interstrand Cross-Linking in Plasmid DNA.* The extent of DNA cross-linking induced by each PBD dimer was determined using the electrophoretic assay method of Hartley et al. (*26*). Closed-circular DNA was linearized with *Hin*dIII, then dephosphorylated, and finally 5′-singly end-labeled using [$\gamma$-$^{32}$P]ATP and polynucleotide kinase. Reactions that included 30−40 ng of DNA were carried out in aqueous TEOA buffer [25 mM triethanolamine and 1 mM EDTA (pH 7.2)] at 37 °C in a final volume of 50 $\mu$L. Reactions were terminated by addition of an equal volume of stop solution (0.6 M NaOAc, 20 mM EDTA, and 100 $\mu$g/mL tRNA) followed by precipitation with ethanol. Following centrifugation, the supernatant was discarded and

the pellet dried by lyophilization. Samples were resuspended in 10 μL of strand separation buffer (30% DMSO, 1 mM EDTA, 0.04% bromophenol blue, and 0.04% xylene cylanol) and denatured by heating to 90 °C for 2.5 min, followed by immersion in an ice/water bath. Control non-denatured samples were resuspended in l0 μL of non-denaturing buffer solution {0.6% sucrose and 0.04% bromophenol blue in aqueous TAE buffer [40 mM Tris, 20 mM acetic acid, and 2 mM EDTA (pH 8.1)]} and loaded directly onto the gel for comparison.

Electrophoresis was carried out for 14−16 h at 40 V using a 0.8% submerged agarose gel (20 cm × 25 cm × 0.5 cm) in TAE buffer. Gels were dried under vacuum for 2 h at 80 °C onto one layer each of Whatman 3MM and DE8I filter papers using a Bio-Rad 583 gel dryer. Autoradiographs were obtained after exposure of Hyperfilm-MP film (Amersham plc) to the dried gel for 4 h with a screen (or overnight, without a screen, to obtain a sharper image). Film bands were quantitated using a Bio-Rad GS-670 imaging laser densitometer. Percentage cross-linking was calculated by measuring the total amount of DNA in each lane [summed density for the double-stranded (DS) and single-stranded (SS) bands] relative to the amount of cross-linked DNA (density of DS band alone). A dose−response curve was derived by plotting the drug concentration against the determined percentage level of cross-linked DNA.

*DNA Cross-Linking in Oligonucleotides.* Single-stranded oligonucleotides (Oligo-1−4 in Figure 3C) were purchased from Pharmacia Biotech and dissolved in deionized water; solutions were stored at −20 °C until they were used. Oligonucleotides were purified, and self-complementary DNA (5 μg) was 5′-end-labeled with [$\gamma$-$^{32}$P]ATP using T4 polynucleotide kinase by the usual procedure. Unincorporated ATP was removed from samples by spinning them through a prewashed Sephadex spin column. For Oligo-4, one strand (2.5 μg) was 5′-labeled before annealing with its complementary strand (2.5 μg). This was carried out by heating to 90 °C for 2 min followed by slow cooling to room temperature. Confirmation that oligonucleotides were in the duplex form was routinely checked using non-denaturing polyacrylamide gels.

Radiolabeled DNA duplex (0.5 μg) was treated with each candidate PBD dimer in a final volume (50 μL) of TEOA buffer. Unless otherwise stated, samples were incubated at 37 °C for 2 h. The DNA was then recovered by ethanol precipitation, washed with 70% (v/v) ethanol, and lyophilized to dryness; the resulting pellet was digested in formamide dye buffer (7 μL). Samples were denatured at 90 °C for 2 min and chilled on ice prior to denaturing PAGE [20% gel, 19:1 (w/w) acrylamide:bisacrylamide ratio, 8.2 M urea, 0.35 mm thick (52 cm × 18 cm)]. Gels were dried under vacuum for 2 h at 80 °C as described in detail above, and finally autoradiographed using Hyperfilm-MP film (Amersham plc). The cross-linked DNA duplex has a reduced mobility compared to the corresponding labeled single strand, and could thus be visualized and quantified using densitometry as described.

*Molecular Models for Interstrand DNA Cross-Linking.* The protocol used for molecular modeling simulations of the cross-linked adducts formed between the PDB dimers and host DNA duplexes has previously been described in detail for the symmetric **2a**−d(CGC***G****ATC***GCG)$_2$ complex (*15*). This three-stage MM/MD/MM methodology was selected to enable a direct comparison of binding energies for the homologous **2a**−**d** PBD dimer series. Briefly, in each case, Verlet molecular dynamics (MD) was performed at 300 K using the Xplor-NIH 2.0.6 (*27*) molecular structure determination package: (i) heating and equilibration to 300 K over the course of 10 ps followed by (ii) 100 ps of production, with coordinate sampling at 1 ps intervals. Averaged coordinate sets were finally relaxed by using Powell molecular mechanics (MM; energy gradient of 0.1 kcal mol$^{-1}$ Å$^{-1}$) to generate the final cross-linked DNA structures.

Initial coordinates for the d(CGCGAT$_m$CGCG)·d(CGCGA$_m$TCGCG) duplexes, where $m = 1-4$, were generated for an idealized B-DNA conformation. These sequences were selected to enable formation of 1,4-, 1,5-, 1,6-, and 1,7-linked adducts where the cross-linked guanine bases positioned on opposite strands are separated by inert A/T stretches of increasing defined length. Starting coordinates for the docked PBD dimers **2a**−**d** were generated by homologous extension of the DSB-120 (**2a**) ligand taken from the reported NMR structural study (*15*). Fully extended, antiperiplanar geometries were used for each drug molecule, with covalent anchoring to the DNA duplex through C11(*S*) linkages in the PBD residues to each of the guanine 2-NH$_2$ groups disposed on opposite strands of the host. This stereochemistry has been shown to be favored for covalent attachment of PBD molecules in the minor groove of duplex DNA (*15*, *16*, *28*). In cases where it was not possible to align a fully extended dimer to achieve covalent contact with the targeted guanines, a G(NH)-PBD-X-PBD monoadduct (where X denotes the diether linkage of the dimer) was first generated by tethering at one end, and an explicit distance restraint was used in the early MD steps of minimization to drive formation toward the target G(NH)-PBD-X-PBD-G(NH) cross-linked structure. This strategy resulted in plausible structures for the cross-linked dimer adducts, particularly for **2b** and **2d**, that were not biased by the energetically unfavorable starting conformations that would otherwise be required for the DNA-bound drug molecules.

Interactive molecular modeling (SYBYL 6.5, from Tripos Inc., St. Louis, MO) and all energy calculations [Xplor-NIH (*27*) with CHARMM parametrization] were carried out on a Silicon Graphics Octane workstation. Force field parameters required for the drug molecules were interpolated from related studies from our laboratories (*15*, *16*, *18*, *28*). Planar restraints were used to maintain planarity for each DNA base, but no artificial terms were required to maintain a Watson−Crick duplex geometry. No attempt was made to influence refinements by restraining either internal or terminal base pairs. Solvent and counterion effects were simulated by using a distance-dependent dielectric constant $\epsilon$ which equals $cr_{ij}$, where $c = 1$ or 4 for the MD and MM step, respectively.

## RESULTS AND DISCUSSION

### *DNA Interstrand Cross-Linking in DNA Oligonucleotide Duplexes*

The PBD monomers (e.g., **1**, DC-81; Figure 1) are known to recognize ∼3 bp of duplex-form DNA with a preference for 5′-Pu-**G**-Pu triplets (Figure 3A). Tethering two such PBDs together would thus be expected to increase the size of the recognition site to ∼6−7 bp, or double that of a

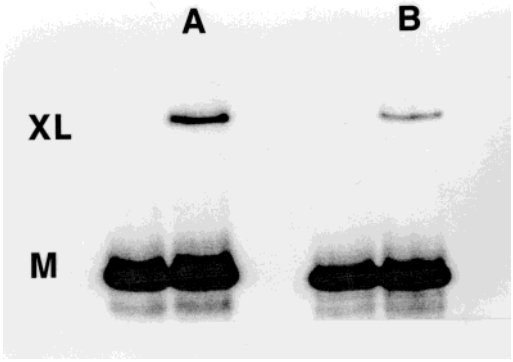


FIGURE 4: Autoradiograph showing interstrand DNA cross-linking in (A) Oligo-1 and (B) Oligo-2 following incubation with **2a** ($n = 3$; 2.5 $\mu$M) at 37 °C for 4 h. Cross-linked duplex DNA (XL) has a lower mobility through the gel than the denatured DNA single-stranded form (M). Control DNA is run beside each drug-treated sample to ensure that non-cross-linked DNA is fully denatured.

monomer subunit. Molecular modeling and solution NMR studies indicate that PBD dimer **2a** ($n = 3$; DSB-120) indeed spans 6 bp (Figures 2A and 3B) and that adenine and thymine are preferred bases in the spanned tract between the two reactive guanines (*10*, *14*, *15*). It was suggested that the more extended PBD dimer **2c** ($n = 5$) should cross-link optimally over a longer sequence, with one further base pair introduced between the two spatially separated and cross-linked guanines. This prediction was assessed by treating a series of 5′-end-labeled duplexes (Figure 3C) with the putative interstrand DNA cross-linking agents **2a**−**d**. The covalent adducts that were generated could be readily visualized and quantitated using denaturing polyacrylamide gel electrophoresis, as cross-linked DNA duplex strands cannot be denatured to the component strands under these conditions (*26*).

*Effect of Bases between the Reactive Guanines.* In Oligo-1 and Oligo-2, two I·C (I is inosine rather than G) pairings are used to flank the core reactive 5′-**G**ATC and 5′-**G**TAC tracts, respectively, to prevent alkylation from occurring at nontargeted G-$NH_2$ sites while retaining thermal stability in such short 10-mer duplexes. Terminal G·C pairings were retained to prevent strand fraying under the experimental temperatures used in the electrophoretic assays. This limitation was avoided in studies of core base complexion (next section) as the longer 12/13-mer duplexes that were used were inherently stable.

Figure 4 shows a gel autoradiograph for Oligo-1 (panel A) and Oligo-2 (panel B) after exposure to PBD dimer **2a** ($n = 3$) for 4 h at 37 °C. Analysis of the gel autoradiograph by densitometry indicates that Oligo-1 is cross-linked ~2-fold more efficiently than Oligo-2, with 8.4 and 4% levels of cross-linking, respectively, for each duplex under the conditions that were used. The 5′-GATC tract is thus more reactive than the reversed 5′-GTAC sequence, in accord with the 5′-**G**-pu > 5′-**G**-py ranking predicted for PBD alkylation from DNA footprinting and molecular modeling studies (*1*, *15*, *16*). This behavior is due to favorable hydrogen bonding between the N10-H10 proton of each bound PBD moiety and the N3 ring nitrogen of 3′-side adjacent adenines (*15*), as shown in Figure 2.

*Effect of the Number of Bases between the Reactive Guanines.* Figure 5 shows a gel autoradiograph in which Oligo-3 and Oligo-4 (Figure 3C) were exposed to **2a**−**d** for 4 h at 37 °C. PBD dimer **2a** ($n = 3$) effectively cross-links Oligo-3 (5′-TATA***G****ATC*TATA) where two base pairs separate the targeted guanines, but does not cross-link Oligo-4 [5′-TATA***G****A(T/A)TC*TATA] where the spanned tract includes an additional A·T base pair. In marked contrast, dimer **2c** ($n = 5$) not only cross-links the longer Oligo-4 sequence but also, to a lesser extent, cross-links the shorter Oligo-3 sequence. Quantitation of the autoradiographs by densitometry showed differences in the level of interstrand cross-linking of Oligo-3 by **2a** (25%) and **2c** (3%). Under equivalent conditions, only 5% of the longer Oligo-4 duplex is cross-linked by **2c**. Both dimer **2b** ($n = 4$) and **2d** ($n = 6$) are ineffective at generating interstrand DNA cross-links with either oligonucleotide under these conditions. In Figure 5 (left panel), an additional band is observed minimally retarded above the single-stranded DNA in lanes marked $n = 4-6$. The nature of this band is unclear, but it may be due to a small extent of monoalkylation of this oligonucleotide

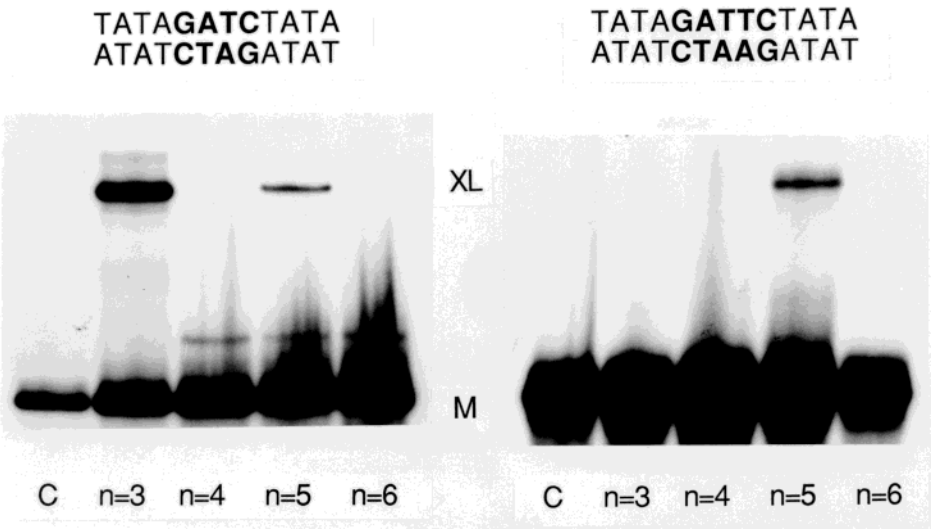


FIGURE 5: Autoradiograph showing cross-linking of Oligo-3 (left) and Oligo-4 (right) by PBD dimers **2a**−**d** ($n = 3-6$, respectively). Reactions were performed with 0.5 $\mu$M drug for 4 h at 37 °C. The cross-linked DNA duplex (XL) has a lower electrophoretic mobility than the denatured, single-stranded DNA (M).

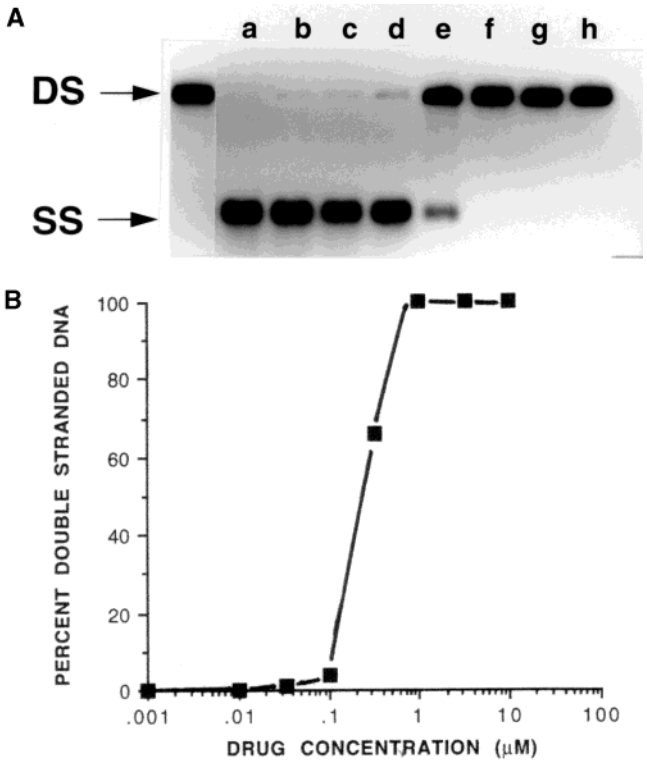


FIGURE 6: (A) Autoradiograph of a representative agarose gel showing interstrand DNA cross-linking by **2c** ($n = 5$) in linear plasmid DNA. Drug treatments were for 2 h at (a) 0, (b) 0.01, (c) 0.033, (d) 0.1, (e) 0.33, (f) 1.0, (g) 3.3, and (h) 10 $\mu$M at 37 °C. (B) Double-stranded (DS) and single-stranded (SS) DNA bands were quantified by laser densitometry to obtain a dose−response curve.

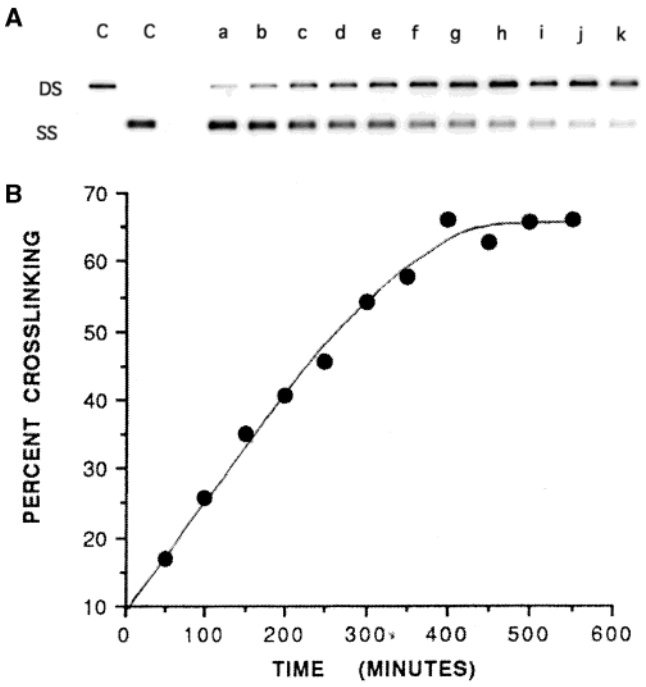


FIGURE 7: (A) Autoradiograph of an agarose gel showing DNA interstrand cross-linking by **2c** ($n = 5$) in linear plasmid pBR322 DNA. Treatments were carried out at 37 °C with 0.14 $\mu$M drug for the indicated times: (a) 50, (b) 100, (c) 150, (d) 200, (e) 250, (f) 300, (g) 350, (h) 400, (i) 450, (j) 500, and (k) 550 min. C indicates drug-free control lanes. (B) Time course profile obtained by quantitative laser densitometry of the double-stranded (DS, i.e., cross-linked duplex) and single-stranded (SS) DNA bands.

by these compounds.

*Effect of Flanking Bases.* Figure 3C shows that the Oligo-1 and -3 contain the optimal 5′-**G**ATC cross-linking site predicted for cross-linking by **2a** (*15*), but the duplexes differ in terms of the sequences flanking the target core. Electrophoretic assay and quantitative analysis revealed the following sequence preference for cross-linking by **2a**: Oligo-3 > Oligo-1. This finding is consistent with observations from DNA footprinting experiments with monomeric PBD agents that 5′-pu-**G** is favored over 5′-py-**G**, and confirms our predictions from extended molecular modeling studies (*15*, *16*).

### *DNA Cross-Linking in Linear Plasmid DNA*

*Cross-Linking Efficiency in Linear pBR322 DNA.* Cross-linking efficiency by dimers **2a**−**d** ($n = 3$−6, respectively) was investigated using the agarose gel electrophoresis assay based on the principle that, following complete denaturation of linear pBR322 DNA (~4300 bp) to the single-stranded (SS) form, an interstrand cross-link results in renaturation to the double-stranded (DS) form in a neutral gel (*26*). Reactions were carried out at 37 °C for 2 h. The resultant bands on the autoradiographs (e.g., Figure 6A) were then analyzed and quantitated by densitometry to calculate the percent of total cross-linked DNA. A dose−response curve can be derived (e.g., Figure 6B), and the concentration that results in 50% cross-linked plasmid DNA ($C_{50}$) can be used as a measure of relative cross-linking ability under the conditions employed. All compounds caused significant DNA cross-linking with a $n = 3 > n = 5 > n = 6 > n =$ 4 order of efficiency, where the even $n$ value homologues were at least 10-fold less efficient than their odd $n$ value counterparts (Table 1). The $n = 3$ and 5 dimers were 400- and 300-fold more efficient than the clinical anticancer agent melphalan, respectively, using identical reaction conditions.

Table 1: DNA Reactivity and Cross-Linking Efficiency of the Homologous PBD Dimers **2a**−**d**, Melphalan, and DC-81 with Plasmid pBR322 DNA[a]

| compound | $n$ | $\Delta T_m$ (°C)[b] | $C_{50}$ ($\mu$M)[c] | cross-linking rate (percent cross-linking $h^{-1}$ $\mu M^{-1}$)[d] |
|---|---|---|---|---|
| DC-81 | − | 0.7 | na[e] | na[e] |
| **2a** | 3 | 15.4 | 0.055 | 108 ± 22 |
| **2b** | 4 | 4.3 | 1.0 | 10.3 ± 4.5 |
| **2c** | 5 | 9.4 | 0.07 | 81 ± 15 |
| **2d** | 6 | 7.1 | 0.75 | 23 ± 12 |
| melphalan | − | nd[f] | 20 | 0.9 ± 0.3 |

[a] Plasmid DNA was incubated with each drug at 37 °C (see text). [b] Thermal stabilization of double-stranded calf thymus DNA after incubation at 37 °C for 18 h (data taken from ref *12*). [c] Drug dose required to induce 50% cross-linking of the DNA following incubation with drug for 2 h. Mean value from at least three experiments. [d] Mean and standard deviation from at least three independent experiments. [e] Not applicable. [f] Not determined.

*Rates of Cross-Linking in Plasmid DNA.* The rates of cross-link formation in linear plasmid pBR322 DNA were measured using the agarose gel assay described herein. Drug concentrations were selected for each compound that induced <100% of the plasmid DNA molecules to be cross-linked. Treatments were continuous at 37 °C, and aliquots from a single reaction mixture were removed (and stopped) at suitable time intervals; all samples were then run simultaneously on a neutral agarose gel. Figure 7A provides a

Table 2: Interaction Energies for Covalent Cross-Linking of d(CGC*GAT*$_m$CGCG)·d(CGC*GA*$_m$*TC*GCG) Duplexes by the Homologous PBD Dimers

| | $E_{bond}$, net bonding energy[a] for bonding sequence | | | |
|---|---|---|---|---|
| PBD dimer | 1,4-link ($m = 1$), 5′-**G**$^1$ATC | 1,5-link ($m = 2$), 5′-**G**$^1$ATTC (=5′-**G**$^5$AATC) | 1,6-link ($m = 3$), 5′-**G**$^1$ATTTC (=5′-**G**$^6$AAATC) | 1,7-link ($m = 4$), 5′-**G**$^1$ATTTTC (=5′-**G**$^7$AAAATC) |
| **2a** ($n = 3$) | **−70.7**[b] | 0.3 | 8.2 | 4.5 |
| **2b** ($n = 4$) | 3.8 | −8.4 | −9.9 | −11.3 |
| **2c** ($n = 5$) | **−43.4** | **−63.3** | −16.6 | −13.8 |
| **2d** ($n = 6$) | −8.2 | −9.9 | −11.4 | −17.6 |

[a] Net bonding enthalpy (kcal mol$^{-1}$) calculated using $E_{complex} - (E_{DNA} + E_{dimer})$, following Xplor-NIH minimization (see Materials and Methods). Significant cross-linking energy terms are highlighted in bold. [b] A value of −73.1 kcal mol$^{-1}$ was determined for the symmetric **2a**−d(CIC***GATC***ICG)$_2$ adduct (*15*).

representative autoradiograph of a gel showing increased cross-linking over time by PBD dimer **2c** ($n = 5$), together with the derived time course plot (Figure 7B). Both **2a** and **2c** cross-linked the plasmid DNA rapidly with a plateau being reached at ∼4.5 and ∼6.5 h, respectively. In contrast, homologous dimers **2b** and **2d** showed a slower rate of cross-link formation and did not achieve plateau levels until 16 and 18 h, respectively. The peak level of DNA cross-linking by melphalan occurred after treatment for 6 h under the same conditions (data not shown).

Each experiment was repeated at least three times, and a direct comparison was made between the cross-linking efficiencies of the four PBD dimers by calculating the percentage level of DNA cross-linked per hour per micromole (Table 1). The results show that **2a** ($n = 3$) cross-links DNA the most rapidly, and that the ranking order of efficiency parallels that for (i) cross-linking ability determined as $C_{50}$ at 2 h, and (ii) drug-induced stabilization of duplex-form calf thymus DNA ($\Delta T_m$). Interestingly, this behavior also correlates with the rank order of cytotoxicity in human leukemic K562 cells ($IC_{50}$ values of 0.2, 2.5, 0.5, and 1.0 $\mu$M for **2a**−**d**, respectively) but does not correlate exactly in other cell lines (*12*).

### *Molecular Modeling of Interstrand DNA Cross-Link Formation*

We have previously used molecular modeling methods to investigate the reactivity and sequence recognition properties of PBD monomers and dimers toward defined DNA target sequences (*15*, *16*, *28*). This approach can provide detailed information about the covalent alkylation events and the underlying structural and energetic factors that dictate reaction profiles. Thus, dynamic modeling has been used to examine the binding energetics of the cross-linking of the [d(CIC***GATC***IGC)]$_2$ duplex by **2a** (DSB-120), and the solution NMR structure of the formed adduct has been determined using NOE-driven annealing methods (*15*).

In this study, molecular modeling has been used to examine the reaction of the homologous PBD dimer series **2a**−**d** with d(CGC**G**AT$_m$CGCG)·d(CGC**G**A$_m$TCGCG) duplexes, where $m = 1-4$. These sequences were selected to establish the effect of inter-guanine distance upon the formation of interstrand DNA cross-links, where the indicated guanines are separated by increasing numbers of inert A·T base pairs. The embedded 5′-***GATC*** duplex tract has been shown to be optimal for reaction with PBD dimer **2a**, as the spanned 3′-side adenine on each strand stabilizes the formed covalent adduct through strong intramolecular A(N3)···H10-N10 hydrogen bonding (see Figure 2) (*15*). This prediction of sequence context for a covalently modified guanine is confirmed by the reactivity profiles obtained for the PBD dimers (see above). The protocol used for molecular modeling and energy calculations was adopted from our earlier studies to enable comparison with reported findings for monoalkylation and sequence-dependent binding behaviors (*15*, *16*, *28*).

The interaction energies determined for the interstrand cross-linking reactions of PBD dimers **2a**−**d** with the defined d(CGC**G**AT$_m$CGCG)·d(CGC**G**A$_m$TCGCG) duplexes are collected in Table 2. It is apparent that only **2a** and **2c** (where $n = 3$ and 5, respectively) form energetically favorable adducts with the DNA hosts, and that the reactivity is inherently dictated by the spatial distribution of the PBD subunits. Thus, dimer **2a** ($n = 3$) only forms a cross-linked adduct with an embedded duplex 5′-GATC tract (i.e., 1,4-link; Figure 8A), but further separation of the guanine sites is disfavored. Inspection of the energy terms (not shown) reveals that marked unfavorable distortion of the duplex through axial bending in the minor groove is required for simultaneous alkylation of opposite-strand guanines by **2a** for the longer 5′-GAT$_{2-4}$C tracts. In the case of **2b** and **2d** ($n = 4$ and 6, respectively), the unfavorable energy terms are primarily a consequence of poor geometry in the -O(CH$_2$)$_n$O- diether linkage that mitigate effective cross-linking of the guanines, particularly for shorter targets, leading to distortion of the host DNA and a poor conformation adopted by the ligand molecules. Interestingly, dimer **2c** ($n = 5$) is unique in that this more extended molecule is able to form cross-linked adducts with both the short 5′-GATC (1,4-link) and the longer 5′-GATTC (1,5-link; Figure 8B) target tracts, although the latter adduct is superior in energy (−43.4 and −63.3 kcal mol$^{-1}$, respectively) due to the more favorable fully extended conformation adopted by the -O(CH$_2$)$_n$O- linkage. The linker group is snugly held by the hydrophobic walls of the DNA minor groove in the case of 5′-GATTC, but is partly displaced away from the helix and compacted by internal conformational rotation to achieve cross-linking within the shorter 5′-GATC tract. Finally, neither 5′-GATTTC nor 5′-GATTTTC duplexes (putative 1,6- and 1,7-links, respectively) offer energetically feasible sites for interstrand cross-linking by any PBD dimer in this homologous diether-tethered series.

Neither **2a** nor **2c** significantly perturbs the local minor groove geometry of the host DNA duplex in their respective favored adducts. A structural NMR study of the **2a**−[d(CIC**G**ATCICG)]$_2$ adduct has shown that the minor groove

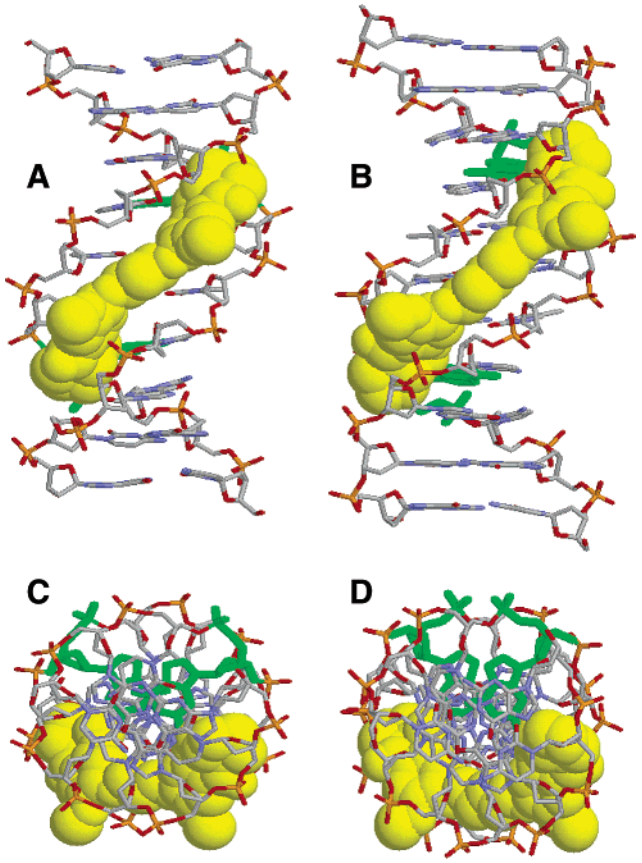


FIGURE 8: Energy-minimized molecular models for the cross-linked structures formed between PBD dimers **2a** ($n = 3$) and **2c** ($n = 5$) and their favored DNA duplex sequences: (A) **2a**−[d(CGC-***G****ATC*GCG)]$_2$ or (B) **2c**−d(CGC***G****ATTC*GCG)·d(CGC***G****AATC*GCG). The top panels (A and B) show the full adducts, viewed looking into the minor groove. The bottom panels (C and D) show the equivalent views looking down the dyad *z*-axis of the duplex. The bound PBD dimers are shown as yellow space-filled representations, and the covalently-modified guanines are highlighted in green. All H-atoms have been removed for clarity. Note the absence of induced helical distortion for the host DNA, and the effective burial of the PBD dimer ligands in the minor groove.

is slightly widened by **2a** in the bonding region upon cross-link formation, with the pliant A/T groove walls making close contacts to effectively "clamp" the bound molecule (*15*). Analogous, but more pronounced, effects have been reported for non-covalent minor groove ligands with A·T preferential binding that occupy similar lengths of duplex, including the antitrypanosomal agents propamidine and pentamidine (*29*−*31*). However, the 5′-A$_{2-3}$T$_{2-3}$ tracts typically required for such ligands are longer than those available in the present 5′-GAT$_{1-2}$C cross-linking sites, where the capping G·C base pairs will confine any drug-induced modulation of local A/T groove width and restrict propagation. The PBD dimers are thus essentially non-distortive with respect to the host DNA, and this behavior will have implications for enzyme repair mechanisms that scan for helical perturbation. Effective burial of **2a** and **2c** within the minor groove, together with minimal drug protrusion from the helical surface (panels C and D of Figure 8, respectively), will present additional difficulties for recognition of the cross-linked lesions.

These results are consistent with findings from the electrophoretic assay and highlight the influence of linker length upon the sequence recognition and cross-linking properties of the PBD dimers (i.e., **2a** > **2c** > **2d** > **2b**). It is notable that the **2b** and **2d** [i.e., even *n* values (2 and 4, respectively)] dimer homologues offer negligible reactivity as interstrand cross-linking agents, and are thus likely to behave as monofunctional PBD agents, as is evident from their poor $\Delta T_m$ values and activity in the gel-based assays (Table 1). In contrast, **2a** and **2c** [i.e., odd *n* values (3 and 5, respectively)] offer a markedly different reactivity profile that is evident from their effects upon the thermal denaturation of duplex-form DNA and the induction of stable interstrand DNA cross-links. The modeling data reported here suggest that shape complementarity and geometry requirements largely dictate the host−drug recognition and cross-linking reactivity profiles.

## CONCLUSIONS

These results illustrate that by altering the linker separation between two covalent binding guanine-targeted PBD moieties, one can recognize discrete sequences of DNA [e.g., 5′-Pu-***G****ATC*-Py or 5′-Pu-***G****A(A/T)TC*-Py in the case of **2a** or **2c**, respectively] through the cross-linking process with a high degree of selectivity. This approach differs from other small molecule approaches to DNA recognition and gene targeting (e.g., hairpin-type polyamides or lexitropsins) that rely upon non-covalent interaction with DNA, and offers the potential to modulate gene expression by blocking transcription in the coding region (*9*).

## REFERENCES

1. Thurston, D. E. (1993) in *Molecular Aspects of Anticancer Drug*−*DNA Interactions* (Neidle, S., and Waring, M. J., Eds.) pp 54−88, The Macmillan Press Ltd., London.
2. Puvvada, M. S., Hartley, J. A., Jenkins, T. C., and Thurston, D. E. (1993) *Nucleic Acids Res. 21*, 3671−3675.
3. Puvvada, M. S., Forrow, S. A., Hartley, J. A., Stephenson, P., Gibson, I., Jenkins, T. C., and Thurston, D. E. (1997) *Biochemistry 36*, 2478−2484.
4. Thurston, D. E., and Bose, D. S. (1994) *Chem. Rev. 94*, 433−465.
5. Kamal, A., Rao, M. V., Laxman, N., Ramesh, G., and Reddy, G. S. K. (2002) *Curr. Med. Chem.: Anti-Cancer Agents 2*, 215−254.
6. Thurston, D. E., Bose, D. S., Howard, P. W., Jenkins, T. C., Leoni, A., Baraldi, P. G., Guiotto, A., Cacciari, B., Kelland, L. R., Foloppe, M. P., and Rault, S. (1999) *J. Med. Chem. 42*, 1951−1964.
7. Gregson, S. J., Howard, P. W., Barcella, S., Nakamya, A., Jenkins, T. C., Kelland, L. R., and Thurston, D. E. (2000) *Bioorg. Med. Chem. Lett. 10*, 1849−1851.
8. Gregson, S. J., Howard, P. W., Corcoran, K. E., Barcella, S., Yasin, M. M., Hurst, A. A., Jenkins, T. C., Kelland, L. R., and Thurston, D. E. (2000) *Bioorg. Med. Chem. Lett. 10*, 1845−1847.
9. Thurston, D. E. (1999) *Br. J. Cancer 80*, 65−85.
10. Bose, D. S., Thompson, A. S., Ching, J. S., Hartley, J. A., Berardini, M. D., Jenkins, T. C., Neidle, S., Hurley, L. H., and Thurston, D. E. (1992) *J. Am. Chem. Soc. 114*, 4939−4941.
11. Thurston, D. E., Bose, D. S., Thompson, A. S., Howard, P. W., Leoni, A., Croker, S. J., Jenkins, T. C., Neidle, S., Hartley, J. A., and Hurley, L. H. (1996) *J. Org. Chem. 61*, 8141−8147.
12. Bose, D. S., Thompson, A. S., Smellie, M., Berardini, M. D., Hartley, J. A., Jenkins, T. C., Neidle, S., and Thurston, D. E. (1992) *Chem. Commun.*, 1518−1520.
13. Smellie, M., Kelland, L. R., Thurston, D. E., Souhami, R. L., and Hartley, J. A. (1994) *Br. J. Cancer 70*, 48−53.
14. Mountzouris, J. A., Wang, J. J., Thurston, D., and Hurley, L. H. (1994) *J. Med. Chem. 37*, 3132−3140.
15. Jenkins, T. C., Hurley, L. H., Neidle, S., and Thurston, D. E. (1994) *J. Med. Chem. 37*, 4529−4537.
16. Adams, L. J., Jenkins, T. C., Banting, L., and Thurston, D. E. (1999) *Pharm. Pharmacol. Commun. 5*, 555−560.

17. Walton, M. I., Goddard, P., Kelland, L. R., Thurston, D. E., and Harrap, K. R. (1996) *Cancer Chemother. Pharmacol. 38*, 431−438.
18. Gregson, S. J., Howard, P. W., Corcoran, K. E., Jenkins, T. C., Kelland, L. R., and Thurston, D. E. (2001) *Bioorg. Med. Chem. Lett. 11*, 2859−2862.
19. Gregson, S. J., Howard, P. W., Hartley, J. A., Brooks, N. A., Adams, L. J., Jenkins, T. C., Kelland, L. R., and Thurston, D. E. (2001) *J. Med. Chem. 44*, 737−748.
20. Gregson, S. J., Howard, P. W., Jenkins, T. C., Kelland, L. R., and Thurston, D. E. (1999) *Chem. Commun*., 797−798.
21. Neidle, S., Puvvada, M. S., and Thurston, D. E. (1994) *Eur. J. Cancer 30A*, 567−568.
22. Neidle, S., and Thurston, D. E. (1994) in *New Targets for Cancer Chemotherapy* (Kerr, D. J., and Workman, P., Eds.) pp 159−175, CRC Press Ltd., Boca Raton, FL.
23. Woynarowski, J. M., Herzig, M. C., Trevino, A. V., Rodriguez, K. A., Hurley, L., and Hardies, S. C. (2001) *Clin. Cancer Res. 7*, 705.
24. Woynarowski, J. M. (2002) *Biochim. Biophys. Acta 1587*, 300−308.
25. Woynarowski, J. M., Hardies, S. C., Trevino, A. V., and Arnett, B. M. (1998) *Ann. Oncol. 9*, 528.
26. Hartley, J. A., Berardini, M. D., and Souhami, R. L. (1991) *Anal. Biochem. 193*, 131−134.
27. Schwieters, C. D,; Kuszewski, J. J., Tjandra, N., and Clore, G. M. (2003) *J. Magn. Reson. 160*, 65−73 (available for academic use from http://nmr.cit.nih.gov/xplor-nih).
28. Adams, L. J., Morris, S. J., Banting, L., Jenkins, T. C., and Thurston, D. E. (1995) *Pharm. Sci. 1*, 151−154.
29. Nunn, C. M., Jenkins, T. C., and Neidle, S. (1993) *Biochemistry 32*, 13838−13843.
30. Jenkins, T. C., and Lane, A. N. (1997) *Biochim. Biophys. Acta 1350*, 189−204.
31. Lane, A. N., Jenkins, T. C., and Frenkiel, T. A. (1997) *Biochim. Biophys. Acta 1350*, 205−220.

BI034313T